Softening and consolidation around seabed pipelines: Centrifuge modelling

Manuscript revised and submitted to *Géotechnique* on 09/03/2017

Michael L. COCJIN (BEng, MEng) (corresponding author)

Centre for Offshore Foundation Systems – M053,

A node of ARC Centre for Geotechnical Science and Engineering

University of Western Australia

35 Stirling Highway, Crawley, Perth, WA 6009, Australia

Tel: +61 8 6488 3995, Fax: +61 8 6488 1044

Email: michael.cocjin@research.uwa.edu.au

Susan M. GOURVENEC (BEng, PhD)

Centre for Offshore Foundation Systems, UWA

A node of the ARC Centre for Geotechnical Science and Engineering

Email: susan.gourvenec@uwa.edu.au

David J. WHITE (MA, MEng, PhD)

Centre for Offshore Foundation Systems, UWA

A node of the ARC Centre for Geotechnical Science and Engineering

Email: david.white@uwa.edu.au

Abstract

Solutions for lateral breakout and axial response of submarine pipelines are well established if the undrained shear strength conditions of the soil are known and defined simply (such as uniform or increasing proportionally with depth). In reality, the geometry of the free surface and the distribution of undrained shear strength around a submarine pipeline post-lay are affected by the lay process. This is because of soil berms that form adjacent to the pipe, and remoulding and subsequent reconsolidation of the seabed. The effect of post-lay consolidation on the subsequent lateral and axial response of submarine pipelines has not been previously investigated through physical model testing.

This paper presents results from centrifuge model tests describing lateral breakout behaviour of a pipe on soft clay as a function of (i) pipe installation conditions, (ii) post-lay pipe weight and (iii) consolidation prior to break out. In addition, the effect of post-lay consolidation on axial pipe response is studied. The experimental results are compared with available numerical and analytical predictions.

The results quantify the influence of the installation process, pipe weight and post-installation consolidation on the lateral break out resistance and trajectory of the pipe and also the axial pipe response, and show how existing prediction methods can capture these effects.

No. of words: 5,393 excluding Abstract

No. of tables: 1

No. of figures: 14

Key words

Pipe, consolidation

Introduction

Networks of in-field pipelines are a central component of offshore subsea developments, creating an increasing need to better understand pipeline behaviour during installation and operation to improve design outcomes.

Offshore in-field pipelines are generally laid directly on the seabed, and left unburied. The pipe partially embeds into the seabed during the laying process due to its self-weight and dynamic lay effects. The lay process submits the soil to disturbance and remoulding, resulting in softening of the seabed deposit surrounding the newly installed pipe. However, after laying, the vertical load on the seabed is reduced to the static pipe weight, and the soil around the pipe consolidates under that load. For the soft, normally consolidated soils typically found offshore, this consolidation process leads to an increase in the strength of the seabed deposit surrounding the pipeline.

The dominant operational forces on deepwater in-field pipelines are from internal temperature and pressure, rather than external hydrodynamic loading. High pipeline temperature causes longitudinal expansion, which is opposed by axial resistance between the pipe and the seabed (Bruton et al. (2008)). Excessive compressive forces arising from thermal expansion or high internal pressure lead to buckling of the pipeline in the lateral direction, with the buckling response depending critically on the soil resistance. Many subsea developments adopt the practice of controlled lateral buckling where a pipeline is allowed to buckle tolerably at designated locations to relieve the thermal and pressure-induced loading (Sinclair et al. (2009)). Lateral buckles along the pipeline can significantly influence the global response of the flowline including the attached infrastructure such as the pipeline end termination or manifolds (PLET/PLEMs).

In recent years, axial and lateral pipe–soil interactions have been studied extensively by researchers, with a particular focus on the undrained conditions that generally prevail during

lateral pipe movements on fine-grained soils. Solutions for penetration, axial and lateral responses using analytical approaches (Randolph and Houlsby (1984), Murff et al. (1989), Martin and Randolph (2006), Randolph and White (2008), Martin and White (2012), Randolph et al. (2012)) and finite element analysis (FEA) both through small-strain (Aubeny et al. (2005), Merifield et al. (2008), Merifield et al. (2009), Krost et al. (2011), Chatterjee et al. (2014)) and large-deformation approaches (Wang et al. (2010), Chatterjee et al. (2012c), Chatterjee et al. (2012a), Chatterjee et al. (2012b), Chatterjee et al. (2013)) are plenty, and can provide a prediction of pipe axial or lateral breakout capacity if the undrained shear strength conditions of the soil are known and defined simply (such as uniform or increasing linearly with depth). Experimental investigations into pipeline behaviour have also been performed at large scale and at reduced scale in a centrifuge, as reported by Bruton et al. (2006), Bruton et al. (2008), Cheuk et al. (2007), Dingle et al. (2008) and Cardoso and Silveira (2010). These studies have led to empirical expressions for the unconsolidated lateral breakout resistance and the subsequent steady residual resistance, simulating a model pipe that breaks out immediately after installation.

In reality, the geometry of the free surface and the distribution of the undrained shear strength around a pipeline post-lay can be significantly affected by the remoulding process during the pipe laying. The axial and lateral resistance subsequently available between the pipeline and the soil is influenced by consolidation of the soil around the pipeline that takes place between the laying process and when the pipeline operation starts. The resulting changes in soil strength and pipe-soil resistance are the subject of this paper. Results of a suite of geotechnical centrifuge tests designed to explore the changes in axial and lateral breakout resistances resulting from installation disturbance and reconsolidation in soft clay are reported and interpreted.

Experimental program

Apparatus

Centrifuge and actuation

The tests were carried out in the 1.8 m radius beam centrifuge at the Centre for Offshore Foundation Systems at the University of Western Australia (Randolph et al. (1991)). The platform of the rotating arm holds a strongbox with dimensions 650 mm by 390 mm in plan and 325 m deep with a maximum payload of 200 kg at 200***g***. Box-mounted actuators control vertical and horizontal loads or displacements of the model through an instrumented loading arm. In-house software is used for control and data acquisition during tests (Gaudin et al. (2009), De Catania et al. (2010)). The tests reported in this chapter were carried out at 25***g***.

Model pipe

A schematic drawing of the model pipe is shown in **Figure 1(a-b)**. The model pipe has a diameter of 30 mm, 150 mm long, representing a diameter of D = 0.75 m and a length of L = 3.75 m at prototype scale. The pipe was fabricated from a solid piece of aluminium with sand glued to the bottom half to provide a rough pipe-soil interface.

The pipe section was instrumented with 6 pore pressure transducers (PPTs) located along the length of the underside of the pipe at the invert and at the sides between the pipe axis and invert. The arc length between the invert and side PPTs is 15.7 mm (0.39 m, prototype scale), forming a central angle of θ_{PPT} = 60°.

Soil sample

To make the model seabed, kaolin clay slurry with water content of 120 % (or twice its liquid limit) was mixed for 2 days in a vacuum. The slurry was poured into the strongbox over a sand

drainage layer covered with a geotextile. The sample was consolidated in-flight, continuously for 65 hours at the test acceleration of 25***g*** to achieve a normally consolidated deposit. Full consolidation was verified via a linearly increasing shear strength profile with depth obtained from ball penetrometer tests. The top of the sample was then scraped to provide a flat and smooth working surface, removing 2-3 mm of clay in the process, leading to a nominal non-zero mudline strength.

A miniature ball penetrometer (Chung and Randolph (2004), Low et al. (2007), Colreavy et al. (2016)) with diameter of 15 mm (0.375 m, prototype scale) was used to measure the shear strength profile of the soil sample. The ball penetrometer was penetrated into the soil sample at a rate of 1 mm/s to ensure undrained conditions (Randolph and Hope (2004)). The first penetration was carried out up to a depth of 88 mm (2.2 m prototype scale), after which 10 cycles of penetration and extraction were carried out between depths 24 mm (0.6 m) and 70 mm (1.75 m) before the penetrometer was completely extracted.

The penetration resistance measured by the ball penetrometer, q_{ball} was corrected for unequal pore pressure and overburden pressure following the expression defined by Chung and Randolph (2004):

$$q_m = q_{ball} - \left[\sigma_{v0} - u_0(1-\alpha)\right]\left[A_s / A_p\right] \qquad 1$$

where q_m is the net penetration resistance, σ_{v0} is the in situ total overburden stress, u_0 is the hydrostatic pressure, A_s/A_P is the ratio of the shaft to the projected area of the ball penetrometer, and parameter α is the net area ratio of the load cell core to the shaft area (equivalent to 0.85 for the tests considered here).

The undrained shear strength, s_u, is back calculated from the net penetration resistance, q_m as:

$$s_u = \frac{1}{N_{ball}}\left(q_m - \frac{F_{buoy}}{A_p}\right) \quad (2)$$

where F_{buoy} is the soil buoyancy force on the ball penetrometer and N_{ball} is the constant ball penetrometer factor, assumed equivalent to 10.5, typical for penetrometer penetration tests (Low et al. (2007), Colreavy et al. (2016)).

The in situ and remoulded shear strength profiles derived from the cyclic ball penetrometer test are shown in **Figure 2(a)** and **Figure 2(b)**, respectively. The shear strength profile was calculated by adopting a constant value for N_{ball} over the entire sample depth, which introduces minimal near-surface error for a normally consolidated soil (Gourvenec et al. (2009), Low et al. (2010)). The resulting intact, in situ, undrained shear strength, s_{u0} was approximated to increase linearly with depth, z within $0 < z$ (mm) < 40 (1 m depth in prototype scale) as:

$$s_{u0} = s_{um} + kz \quad (3)$$

with mudline strength of s_{um} = 0.1 kPa, and strength gradient of k = 0.7 kPa/m. Degradation in shear strength due to remoulding during the cyclic phase of the ball penetrometer test shows a final remoulded strength of the soil, δ_{rem} = 0.47 (**Figure 2(b)**), where δ_{rem} is defined as the ratio of the remoulded to intact strength as measured halfway of the cycled route (z = 47 mm, or 1.175 m in prototype scale). The evolution of the remoulded shear strength with loading cycle shown in **Figure 2(b)** can be captured by the commonly-used exponential degradation curve pattern (Einav and Randolph (2005)) given by:

$$\frac{s_{u,cyc}}{s_{u0}} = \delta_{rem} + \left[1 - (\delta_{rem})\right] e^{\frac{-3(N-0.5)}{N_{95}}} \quad (4)$$

where $s_{u,cyc}$ is the strength measured during the cyclic phase of the ball penetrometer test, and N_{95} = 2.5 is the number of cycles required to achieve 95 % of δ_{rem} from the intact strength.

The moisture content profile of the soil model was also determined from core samples taken after all the tests, where an average effective unit weight, $\gamma' = 5.7$ kN/m^3 over the depth of the soil model was obtained.

Pipe testing programme

A series of pipe tests was carried out, as summarised in **Table 1**. Each test involved initial penetration of the pipe to a depth equal to half the diameter ($w/D = 0.5$) to simulate the installation or pipe 'laying' process. The pipe was then unloaded to an operative vertical load, V_{op}, defined as a proportion of the load, V_{max} achieved at a penetration of $w/D = 0.5$, where V_{op} represents the pipe weight. Unloading ratios, $V_{op}/V_{max} = 1, 0.5, 0.25, 0.125$ were considered as detailed in **Table 1**.

Following installation, axial or lateral breakout of the pipe was simulated immediately, or after a period of consolidation that allowed essentially full dissipation of the excess pore pressures developed during installation. The pipe was translated axially (δy in **Figure 1(b)**) and laterally (δx in **Figure 1(b)**) under constant vertical load, V_{op} allowing the pipe to rise or fall to maintain this load, to assess the breakout resistance.

Two alternative 'laying' methods were considered: undrained monotonic vertical penetration and undrained cyclic installation, simulated by a specified pattern of oscillations, thus remoulding the surrounding soil. The adopted pattern of lateral displacement during the cyclic penetration mimics the disturbance and remoulding associated with a real lay process.

Undrained penetration response

The influence of installation or pipe 'laying' method on the pipe penetration response is presented in **Figure 3**.

The pipe penetration resistance is expressed in terms of the pipe vertical bearing pressure per unit length, V/D, and normalised vertical penetration resistance, V/Ds_{u0}. Profiles with pipe invert embedment, w/D for different tests are shown in **Figure 3(a)** and **Figure 3(b)**, respectively. An inset figure in **Figure 3(a)** shows the pipe displacements during penetration, indicating the trajectory of the monotonically and cyclically penetrated pipe cases.

The monotonic penetration response is highly repeatable as shown in **Figure 3(a–b)**. A linear increase in V/D with depth is observed in these cases, with the response dominated by the linear variation of the undrained shear strength with depth (**Equation** 3). The increase in V/Ds_{u0} with depth on monotonic cases is compared against existing numerical solutions (Aubeny et al. (2005) and Chatterjee et al. (2012a), based on small-strain and large deformation finite element analyses, respectively) as shown in **Figure 3(b)**. At w/D = 0.5, a normalised vertical penetration resistance of V_{max}/Ds_{u0} ~ 10.5 is recorded in the centrifuge tests close to the value derived by Aubeny et al. (2005). The numerical solutions presented in **Figure 3(b)** considers V/Ds_{u0} as a sum of the soil resistance and a component due to buoyancy as the pipe becomes embedded within the soil, expressed as:

$$\frac{V}{Ds_{u0}} = N_c + N_b\left(\frac{\gamma' w}{s_{u0}}\right) \qquad 5$$

where the soil bearing factor, N_c reflects the component of the soil resistance, typically expressed in terms of a power law function of the penetration depth (Aubeny et al. (2005)). The pipe buoyancy resistance, $N_b\gamma' w$ increases with depth as shown in **Figure 3(a)**, where N_b is the self-weight factor given by:

$$N_b = f_b\frac{A_s}{Dw} \qquad 6$$

N_b is proportional to the potential energy needed to lift the displaced soil with a nominal weight of $A_s\gamma'$ to the top of the pre-existing heave next to the pipe, with A_s being the cross-sectional area of the embedded pipe. When the displaced soil forms heave mounds and alters the geometry of the soil next to the pipe, the soil buoyancy is enhanced through the factor f_b where an f_b = 1 corresponds to no heave, following Archimedes' principle (buoyancy force being equal to the weight of the displaced fluid). The effects of buoyancy and the changes in soil geometry and development of soil heave during penetration are not considered in the upper bound plasticity solution presented by Randolph and White (2008) which assumes a flat seabed surface, resulting in lower V/Ds_{u0} estimates compared to the values observed in the current centrifuge tests (**Figure 3(b)**).

Existing solutions do not capture the more complicated penetration response exhibited by cyclically penetrated pipe (**Figure 3(b)**). The cyclic penetration of the pipe mobilised a lower V/D and V/Ds_{u0} compared to monotonically penetrated pipes. The decrease in penetration resistance during the oscillating movements of the pipe is reflected by the elevated pore water pressure in the surrounding soil shown in **Figure 3(c)** which plots the excess pore water pressure at the pipe invert as a ratio of the pipe vertical bearing pressure per unit length, $\Delta u_{inv}/(V/D)$.

Post-lay consolidation response

Figure 4(a) presents the variation with time, t (prototype scale) of the pore water pressure, u, relative to a datum of zero prior to penetration of the pipe, for each of the PPTs installed in the model pipe during penetration, post-lay consolidation, and lateral loading in test R2CU. The average pore pressure recorded by the invert and side PPTs are denoted as u_{inv} and u_{side}, respectively. In general, pore pressure around the pipe increases when the soil is loaded, as V/D increases, and when remoulded via the simulated dynamic lay process. However, pore pressure reduces at constant V/D during post-lay consolidation, during which time the excess pore water

pressure at the pipe invert, Δu_{inv} which is equivalent to the difference between u_0 and the invert pore water pressure, u_{inv} as shown in **Figure 4(b)**, dissipates.

The change in excess pore pressure at the pipe invert level, normalised by the maximum value recorded under the maximum vertical load, is shown in **Figure 5(a)** for various tests, with the time axis zeroed at the moment when the reduction in vertical load is complete. The subsequent unloading from V_{max} to V_{op} is evident in a concurrent drop in excess pore pressure at the invert level.

The influence of pipe weight on the post-lay dissipation behaviour of the invert excess pore pressure is shown more clearly in **Figure 5(b)** which plots Δu_{inv} relative to V/D against time factor, $T = c_v t/D^2$ with c_v being the vertical coefficient of consolidation. At the start of consolidation, the excess pore pressure is higher relative to the applied stress for increasing unloading ratio, V_{max}/V_{op}. The additional excess pore water pressure generated by the cyclic penetration of the pipe is also evident in this figure (compare RemR4CU against R4CU in **Figure 5(b)**).

Figure 5(c) shows that the post-lay dissipation behaviour in pipe cases with $V_{op} > 0.5 \cdot V_{max}$ (R1CU and R2CU) is close to the solutions derived from elasto-plastic (Chatterjee et al. (2012c)), and elastic (Krost et al. (2011)) small-strain FEA models. For pipes at a higher overloading ratio and with remoulding during installation, the additional excess pore pressure created by these effects leads to a higher response. However, with dissipation, all responses converge towards the theoretical solution. The only exception is R8CU, which is an outlier. For this high overloading ratio, only small level of remnant excess pore pressure is needed at the invert to cause a high value of $(\Delta u/\Delta u_{ini})_{inv}$.

The dissipation of excess pore pressure during post-lay consolidation results in an increase in effective stress in the soil around the pipe. The effective stress increase can be illustrated by

defining an effective contact enhancement factor, ζ' given by the ratio of the effective normal force, N' acting around the pipe-soil contact and the pipeline submerged weight per unit length, V (White and Randolph (2007), Krost et al. (2011)) as:

$$\zeta' = \frac{N'}{V} \quad (7)$$

At full consolidation (when the excess pore pressure is completely dissipated), the effective stress is equal to the total stress around the pipe. A total force, N can be obtained by summing the normal contact stresses over the pipe-soil contact perimeter, p and this force exceeds the pipeline submerged weight per unit length, V due to a 'wedging' effect around the curved pipe surface (**Figure 1**(c)). The ratio $\zeta = N/V$ was derived by White and Randolph (2007) following the elastic solution for a line load acting on a half-space, assuming that the normal stress on the pipe wall varies with $\cos\theta$, where θ is the inclination from the vertical. $\zeta = N/V$ can then be obtained as:

$$\zeta = \frac{N}{V} = \frac{2\sin\theta}{\theta + \sin\theta\cos\theta} \quad (8)$$

where $\cos\theta = 1 - 2(w/D)$. Through **Equation** 8, the total force, N acting on the pipe with embedment of $w = 0.5D$ is $1.27V$.

The effective force, N' in **Equation** 7 is determined following the principle of effective stress as:

$$N' = N - p\Delta\bar{u} \quad (9)$$

where $\Delta\bar{u}$ is the average excess pore pressure around the pipe, obtained in this case by linearly interpolating the recorded excess pore pressures at the pipe invert (Δu_{inv}), the side PPTs (Δu_{side}), and the zero pore pressure at the edge of the pipe and soil surface.

The distribution of the total radial stress, σ_r and the interpolated Δu during consolidation, normalised by the prescribed vertical bearing pressure, V/D is shown in **Figure 6(a)** and **Figure**

6(b) for tests R4CU_AX and RemR4CU, respectively. **Figure 6(a)** also includes the distribution of Δu around the pipe in test R4UU_AX just before the pipe was displaced axially. These results are converted to the effective contact enhancement factor, ζ' (**Equation** 7), varying with time factor, $T = c_v t/D^2$ in **Figure 6(c)** where the vertical coefficient of consolidation, c_v (m^2/year) was assumed to vary with stress (in kPa), via the increase in mean effective stress at the pipe-soil contact, N'/p through the form $c_v = (0.3+0.16N'/p)^{0.47}$ (Cocjin et al. (2014)).

Figure 6(c) shows that the elastic small-strain FEA solution by Krost et al. (2011) matches the increase in ζ' with time for the case without vertical unloading (R1CU). In this case, the average excess pore pressure and the effective stress have equal contribution to the total stress immediately after vertical unloading, with the effective stress eventually increasing to total stress with the dissipation of the excess pore pressure. The increase in ζ' with time can be expressed in a form given by **Equation** 10 as:

$$\zeta' = \zeta + \left(\frac{\zeta_{UU} - \zeta}{1 + (T/T_{50})^m} \right) \qquad 10$$

where ζ (**Equation** 10) and ζ_{UU} are the fully consolidated ($T \rightarrow \infty$) and unconsolidated ($T \sim 0$) undrained effective contact enhancement factors.

In **Equation** 10, T_{50} is the time factor when 50 % of the increase in ζ has occurred and m is a constant. **Equation** 10 is plotted in **Figure 6(c)** using m = 1.05, and T_{50} = 0.135 suggested for rough pipe with embedment of $w = 0.5D$ (Chatterjee et al. (2012c)), and matches well the measured trends.

The unconsolidated undrained effective contact enhancement factor, ζ_{UU} reduces with increasing overload ratio, and is reduced further for the case with remoulding during pipe penetration (case RemR4CU). This is because the overloading and remoulding processes both create additional

excess pore pressure, meaning that initially a lower portion of the pipe weight is carried by effective stress. After full dissipation, however, the effective contact enhancement factor returns to the total stress value ($\zeta' = \zeta$), which for w/D = 0.5 is estimated as ζ = 1.27. An important consequence of this effect is that there is a lower axial friction initially available, as discussed in the following section, and **Equation** 10 combined with the observed values of ζ_{UU} provides a basis to estimate the time period over which this evolves.

Axial load-displacement response

Post-lay consolidation effects

The axial friction factor, H_{ax}/V and normalised axial breakout resistance, H_{ax}/Ds_{u0} are plotted against the normalised axial displacement, y/D for test with and without post-lay consolidation (R4CU_AX and R4UU_AX) in **Figure 7(a)** and **Figure 7(b)**, respectively. Consolidation prior to axial breakout results in higher steady-state ('residual') axial resistance, and also a pronounced peak exhibited initially. The peak and residual resistances during axial displacement after post-lay consolidation, when expressed as a friction factor, are 3.5 and 1.6 times greater than the residual resistance with breakout immediately after installation.

Prediction of undrained axial breakout capacity

The increase in axial breakout resistance due to consolidation is directly linked to the effective contact enhancement factor, ζ' (**Equation** 7) where the axial friction factor, H_{ax}/V can be expressed as:

$$\frac{H_{ax}}{V} = \zeta' \tan\delta \qquad 11$$

where δ is the pipe-soil friction angle. Using the excess pore pressure prior to axial loading, **Equation** 11 provides a good prediction to the observed axial residual resistance on both the

consolidated and unconsolidated cases, assuming a pipe-soil friction angle of $\delta = 27.5°$, which is typical for kaolin at low stresses (Hill et al. (2012)).

Lateral load-displacement response

Installation and post-lay consolidation effects

The effect of post-lay consolidation and pipe 'laying' method on the lateral load-displacement response is shown in **Figure 8(a)** and **Figure 8(b)** which plot the normalised lateral resistance, H/Ds_{u0} and lateral friction factor, H/V against the normalised lateral displacement, x/D for tests with V_{op}/V_{max} = 0.25 (R4 series). V/Ds_{u0} and w/D during the lateral displacement of the pipe are correspondingly provided in **Figure 8(c)** and **Figure 8(d)**. Although the tests took place with a constant simulated pipe weight, V/Ds_{u0} increases as the pipe rises, reflecting the reduction in in situ soil strength at the pipe invert level.

The lateral response after post-lay consolidation exhibited higher resistance than the case without post-lay consolidation (compare R4CU and R4UU in **Figure 8(a–b)**). An immediate peak was recorded during lateral breakout following consolidation, similar to the observations made on the axial breakout response shown in **Figure 7(a–b)**. An improvement in lateral resistance due to consolidation is observed within ~ 0.6D lateral distance from the as-laid location (**Figure 8(a–b)**). The breakout resistance is 1.8 times greater with post-lay consolidation than without, after which the lateral resistance (H/Ds_{u0} and H/V) on both the consolidated and unconsolidated cases converge to a similar value as the pipe moves further away from the as-laid position, encountering soil unaffected by the post-lay consolidation. The gain in lateral resistance due to post-lay consolidation is also higher for the pipe that was cyclically installed than in the pipe that followed monotonic penetration (compare R4CU against RemR4CU in **Figure 8(a–b)**). Cyclic remoulding of soil during pipe laying also created a wider zone of strengthened soil, where enhancement of resistance can be observed up to 0.75D lateral distance from the installation

location (although the test was terminated shortly afterwards). Cyclic remoulding of soil during pipe laying led to elevated levels of excess pore pressure (**Figure 3(c)**) that consequently resulted in a greater reduction in moisture content and therefore strengthening after dissipation.

The observed differences in breakout resistance are consistent with the excess pore pressure recorded at the PPT on the rear side of the pipe, Δu_{rear} shown in **Figure 8(e)**. Higher negative pore pressure is observed for the higher breakout resistance, but in all cases the excess pore pressure is lost after approximately 0.5 diameters of movement, when a gap at the rear of the pipe causes pore pressures at the PPT location to become hydrostatic. The outcome – which is initially counter-intuitive – arises as more softening during pipe laying resulted in more net hardening after consolidation.

Comparison with theoretical solutions for unconsolidated, undrained lateral breakout capacity

The effect of pipe weight on the lateral breakout resistance for cases without post-lay consolidation is assessed through failure envelopes defining the combination of vertical and lateral loads in **Figure 9**. The unconsolidated undrained lateral breakout capacity, indicated by the individual data markers, is defined as the maximum resistance recorded during the lateral displacement of the pipe, and occurred after $x \sim 0.3D$. Unconsolidated undrained failure envelopes in $V/Ds_{u0} - H/Ds_{u0}$ and $H/V - V/V_{ult,UU}$ load spaces are shown on **Figure 9(a)** and **Figure 9(b)**, respectively. These are based on the upper bound plasticity solution by Randolph and White (2008) for weightless soil, and numerical limit analysis by Martin and White (2012) for weighty soil. In both cases the pipe is assumed to be fully rough, wished-in-place and at an embedment of $w/D = 0.5$ in a soil with strength proportional to depth. Both solutions underestimate the unconsolidated undrained lateral breakout capacity observed in the present set of centrifuge test results, which is attributed to the neglect of heave and soil berms as earlier

demonstrated in **Figure 3(b)**, noting that this penetration resistance would determine the size of the failure envelope in the lateral load dimension.

The formation of soil heave beside the pipe during penetration is shown in **Figure 10** through a sequence of underwater photographs taken during a pipe test. This heave results in an additional embedment, and provides additional resistance during lateral breakout as the pipe mobilises a greater volume of soil. The effect of the heave can be estimated by considering the volume of the soil displaced by the pipe during penetration. Dingle et al. (2008), through observations of the changes in soil surface profiles during pipe penetration using image analyses, estimated the effective increase in embedment, Δw_{heave} as:

$$\frac{\Delta w_{heave}}{D} = \frac{1}{8}\frac{D}{(0.8D')}\left[\sin^{-1}\left(\frac{D'}{D}\right) - \frac{D'}{D}\sqrt{1-\left(\frac{D'}{D}\right)^2}\right] \qquad 12$$

where $D' = 2D[(w/D) - (w/D)^2]^{0.5}$. An effective embedment of ~ $0.7D$ for a pipe penetrated to $w = 0.5D$ is derived through **Equation** 12. The unconsolidated undrained failure envelope corresponding to this effective embedment using the limit analysis solution by Martin and White (2012) predicts well the lateral breakout capacity observed in the present set of centrifuge test results shown in **Figure 9**.

Comparison with theoretical solutions for the consolidated, undrained lateral breakout capacity

The effect of pipe weight on the lateral breakout resistance for cases with post-lay consolidation is assessed through failure envelopes in **Figure 11**.

The consolidated undrained lateral breakout capacity, indicated by individual data markers, is defined as the peak resistance recorded during the immediate lateral displacement of the pipe, and occurred during $x \sim 0.01D$, which is a smaller displacement than for the unconsolidated cases.

The consolidated undrained failure envelope is derived by scaling the unconsolidated undrained envelope as a function of the increase in the undrained shear strength due to consolidation, Δs_u using an approach set out by Gourvenec et al. (2014) for shallow foundations. The mobilised soil below the pipe is lumped as a single element for which the operative increment in consolidation stress due to the preload can be estimated for initially normally consolidated conditions as:

$$\Delta\sigma'_c = f_\sigma\left(\frac{N}{D}\right) \qquad 13$$

where N is the enhanced normal force that takes into account the wedging effect around the pipe as defined by **Equation** 8 (Chatterjee et al. (2014)), whilst the factor f_σ takes into account the non-uniform distribution of the stress in the affected zone of soil. The resulting increase in strength of the soil affected by consolidation is then calculated as:

$$\Delta s_u = f_{su}\Delta\sigma'_c\left(\frac{s_u}{\sigma'_v}\right)_{NC} \qquad 14$$

where the shear strength factor f_{su} scales the gain in strength of the 'lumped' soil to that mobilised during subsequent failure, and $(s_u/\sigma'_v)_{NC}$ is the normally consolidated strength ratio of the soil, equivalent to 0.15 in the present test conditions.

The consolidated undrained vertical and lateral breakout capacities are assumed to scale with the increase in the undrained shear strength in the form:

$$\frac{V_{ult,CU}}{V_{ult,UU}} = 1+\frac{\Delta s_u}{s_{u0}} = 1+ f_{su(V)}f_\sigma\left(\frac{s_u}{\sigma'_v}\right)_{NC}\left(\frac{V}{Ds_{u0}}\right)_{UU} \qquad 15$$

$$\frac{H_{ult,CU}}{H_{ult,UU}} = 1+\frac{\Delta s_u}{s_{u0}} = 1+ f_{su(H)}f_\sigma\left(\frac{s_u}{\sigma'_v}\right)_{NC}\left(\frac{V}{Ds_{u0}}\right)_{UU} \qquad 16$$

where $(V/Ds_{u0})_{UU}$ is the normalised unconsolidated undrained vertical pipe resistance mobilised at the effective embedment. Separate scaling factors, f_σ and f_{su} in **Equations** 15 - 16 allow the response in the overconsolidated conditions to be captured, but in the present normally consolidated conditions, there is effectively a single scaling parameter, $f_\sigma f_{su}$ for a particular load path. The increase in the vertical and lateral breakout capacities through consolidation as observed in the present set of centrifuge test results is predicted well through **Equations** 15 - 16 using the scaling parameters $f_\sigma f_{su(V)} = 0.439$ derived in FEA studies carried out by Chatterjee et al. (2014) for pipe, and $f_\sigma f_{su(H)} = 0.919$ derived by Feng and Gourvenec (2015) as shown in **Figure 11.** The results demonstrate that the expansion of the failure envelopes through consolidation is captured well by the theoretical framework outlined by Gourvenec et al. (2014), where the increase in operative soil strength is linked to the pipe weight. The observed increase in lateral breakout capacity, H_{ult}, due to consolidation is higher than the predicted gain in vertical pipe capacity, V_{ult}, consistent with analysis of mudmat foundations (Feng and Gourvenec (2015)). For the load levels used in the model test cases, the theoretical envelope and the experimental results show gains in lateral breakout capacity of 20% - 50% (**Figure 11**).

Pipe trajectory

The effect of post-lay consolidation and installation or pipe 'laying' method on the pipe trajectory during subsequent axial and lateral loading is summarised in **Figure 12**. The figure plots the normalised pipe embedment at the invert level, w/D against the normalised axial displacement, y/D and normalised lateral displacement, x/D for tests with $V_{op}/V_{max} = 0.25$ (R4 series). Overall, the trajectory is approximately the same with the pipe moving upwards as expected for the pipe weight relative to the vertical bearing capacity, at a slope of ~ 1° and ~ 10° during axial and lateral displacements, respectively. When the pipe is loaded axially or laterally immediately after

the installation, larger upward displacements were recorded than during the movement of pipe after a period of post-lay consolidation.

The effect of pipe weight on the pipe trajectory during lateral loading is shown in **Figure 13**. The present centrifuge response is compared against LDFE analysis results reported in Wang et al. (2010), where the general behaviour between two set of results is similar with lighter pipes ($V_{op} < 0.5V_{max}$) rising from breakout embedment during lateral displacement, and heavier pipes moving downward penetrating deeper into the soil with increasing lateral displacement, *x/D*.

The direction of pipe displacement during lateral breakout at failure, $\delta w/\delta x$, for varying V_{op}/V_{max} can be directly assessed by assuming an associated flow rule (or normality), where $\delta w/\delta u$ at failure can be assumed normal to the failure envelope defined in the *V-H* load space. Recorded $\delta w/\delta x$ for a given V_{op}/V_{max} obtained in the centrifuge tests are compared against existing solutions in **Figure 14(a)** and **Figure 14(b)** for cases without and with post-lay consolidation.

In general, $\delta w/\delta x$ observed in the centrifuge tests for $V_{op} < 0.5 \cdot V_{max}$ on pipe with and without post-lay consolidation agrees closely with existing solutions based on large-deformation FEA estimates (Wang et al. (2010)), and based on limit analysis after accounting for the effective embedment as discussed above (Martin and White (2012)). However, both solutions slightly over predict $\delta w/\delta x$ for $V_{op} > 0.5 \cdot V_{max}$.

Concluding remarks

This paper has presented results of a centrifuge test programme that investigated the influence of installation or laying method, and post-lay consolidation on the axial and lateral breakout response of a pipeline section on a normally consolidated soil.

Different initial conditions involving varying levels of generation and dissipation of excess pore pressure during pipe installation, and operative vertical loads (representing a range of pipe

weight) were explored. Axial and lateral breakout response of the pipe was assessed under undrained loading conditions immediately after installation, or after a period of consolidation to allow essentially full dissipation of the excess pore pressures developed during installation.

The results showed a strong installation effect. This effect results from post-laying consolidation, and is enhanced if the lay process involves remoulding. Four key conclusions emerge following the observations made:

- After pipeline installation, the strength of the surrounding soil can be significantly enhanced due to consolidation under the pipe self-weight.
- Cyclic pipe movements or oscillations during installation create additional excess pore pressure in the soil surround the pipeline. Although this remoulding weakens the soil in the short term, the subsequent strength gain during consolidation is greater than following monotonic installation.
- The axial and lateral breakout resistance is significantly enhanced by these changes in strength – by 20% - 50% for the cases in this study. The relevant operative strength should be used with existing solutions to estimate breakout resistance. A theoretical framework and numerically derived scaling factors were presented for the pipeline conditions considered in this study.
- The penetration of the pipe results in additional embedment due to the development of soil heave next to the embedded pipe. This additional effective embedment results in additional breakout resistance, and existing numerical and analytical solutions based on wished-in-place (no heave) conditions should be modified using the effective embedment. When the solutions are applied in this way, in combination with the in situ soil strength, the response is predicted well.

These results illustrate how the installation process and post-installation consolidation effects combine to alter the soil strength around a seabed pipeline, and show how existing prediction methods can capture these effects.

Acknowledgements

The work described here forms part of the activities of the Centre for Offshore Foundation Systems, currently supported as a node of the Australian Research Council Centre of Excellence for Geotechnical Science and Engineering. This support is gratefully acknowledged. The technical support provided by beam centrifuge technician, Mr. Manuel Palacios is also gratefully acknowledged. The third author acknowledges the support of the Shell EMI Chair in Offshore Engineering, at UWA.

Notations

The following symbols were used in the paper.

D	pipe diameter
L	pipe length
$(s_u/\sigma'_v)_{NC}$	normally consolidated strength ratio
$(V/Ds_{u0})_{UU}$	normalised unconsolidated undrained vertical pipe resistance mobilised at the effective embedment
A_s/A_P	ratio of the shaft to the projected area of the ball penetrometer
c_v	vertical coefficient of consolidation
D'	effective contact width of the pipe
f_b	soil buoyance enhancement factor
F_{buoy}	soil buoyancy force on the ball penetrometer
f_σ	stress factor
f_{su}	strength factor
H/Ds_{u0}	normalised lateral resistance
H/V	lateral friction factor
H_{ax}	axial horizontal load
H_{ax}/Ds_{u0}	normalised axial breakout resistance
H_{ax}/V	axial friction factor
k	undrained shear strength gradient
m	constant
N'	effective normal force around the pipe-soil contact
N_{95}	number of cycles required to achieve 95% of fully remoulded strength from the intact strength
N_b	self-weight factor
N_{ball}	ball penetrometer factor
N_c	soil bearing factor reflecting the soil resistance component
p	pipe-soil contact perimeter
q_{ball}	penetration resistance measured by the ball penetrometer
q_m	net penetration resistance of the ball penetrometer

s_u	undrained shear strength
$s_{u,cyc}$	cyclic/remoulded undrained shear strength
s_{u0}	intact, in situ, undrained shear strength
s_{um}	mudline undrained shear strength
T	non-dimensional time factor
t	time
T_{50}	time factor when 50 % of the increase in total contact enhancement factor, ζ has occurred
u	pore pressure
u_0	hydrostatic pressure
u_{inv}	pore pressure at the pipe invert (averaged)
u_{side}	pore pressure at the side pore pressure transducers (averaged)
V/D	pipe vertical bearing pressure per unit length
V/Ds_{u0}	normalised vertical penetration resistance
V_{max}	vertical load at a penetration of $w/D = 0.5$
V_{op}	operative vertical load
V_{op}/V_{max}	unloading ratio
$V_{ult,CU}$	consolidated undrained ultimate vertical load capacity
$V_{ult,UU}$	unconsolidated undrained ultimate vertical load capacity
w	pipe penetration at the invert level
x	lateral displacement
x/D	normalised lateral displacement
y	axial displacement
y/D	normalised axial displacement
z	depth
α	net area ratio of the load cell core to the shaft area
δ	pipe-soil friction angle
δ_{rem}	final remoulded strength of the soil
Δs_u	increase in the undrained shear strength due to consolidation
Δu	excess pore pressure around the pipe

$\Delta\bar{u}$	sum of excess pore pressure around the pipe (averaged)
Δu_{inv}	excess pore pressure at the pipe invert (averaged)
Δu_{rear}	excess pore pressure at the rear side of the pipe (averaged)
Δu_{side}	excess pore pressure at the side pore pressure transducers (averaged)
Δw_{heave}	effective increase in embedment due to soil heave
γ'	average effective unit weight of the soil
θ	inclination from the vertical of the vertical load acting on the pipe
θ'	half of the central angle formed by the effective contact width of the pipe
θ_{PPT}	central angle of side-to-side pore pressure transducers
σ_r	total radial stress
σ_{v0}	in situ total overburden stress
ζ	total contact enhancement factor/fully consolidated undrained effective contact enhancement factor
ζ'	effective contact enhancement factor
ζ_{UU}	unconsolidated undrained effective contact enhancement factor

460

References

Aubeny, C. P., Shi, H. & Murff, J. D. (2005) Collapse Loads for a Cylinder Embedded in Trench in Cohesive Soil. *International Journal of Geomechanics* **5(4)**:320-325.

Bruton, D., White, D., Cheuk, C., Bolton, M. & Carr, M. (2006) Pipe/Soil Interaction Behavior During Lateral Buckling, Including Large-Amplitude Cyclic Displacement Tests by the Safebuck JIP. In *Offshore Technology Conference*.) Offshore Technology Conference, Houston.

Bruton, D. a. S., White, D. J., Carr, M., Cheuk, J. C. Y. & Kong, H. (2008) Pipe-Soil Interaction During Lateral Buckling and Pipeline Walking — The SAFEBUCK JIP. *Proc. Offshore Technol. Conf., Houston, TX, Paper OTC19589*.

Cardoso, C. O. & Silveira, R. (2010) Pipe-Soil Interaction Behavior for Pipelines Under Large Displacements on Clay Soils - A Model for Lateral Residual Friction Factor In *Proceedings of Offshore Technology Conference*. Offshore Technology Conference.

Chatterjee, S., Gourvenec, S. & White, D. J. (2014) Assessment of the consolidated breakout response of partially embedded subsea pipelines. *Géotechnique* **64(5)**:391-399.

Chatterjee, S., Randolph, M. F. & White, D. J. (2012a) The effects of penetration rate and strain softening on the vertical penetration resistance of seabed pipelines. *Géotechnique* **62(7)**:573-582.

Chatterjee, S., White, D. & Randolph, M. (2012b) Numerical simulations of pipe-soil interaction during large lateral movements on clay. *Géotechnique* **62(8)**:693-705.

Chatterjee, S., White, D. J. & Randolph, M. F. (2013) Coupled consolidation analysis of pipe–soil interactions. *Canadian Geotechnical Journal* **50(6)**:609-619.

Chatterjee, S., Yan, Y., Randolph, M. & White, D. (2012c) Elastoplastic consolidation beneath shallowly embedded offshore pipelines. *Géotechnique Letters* **2(2)**:73-79.

Cheuk, C. Y., White, D. J. & Bolton, M. D. (2007) Large-scale modelling of soil–pipe interaction during large amplitude cyclic movements of partially embedded pipelines. *Canadian Geotechnical Journal* **44(8)**:977-996.

Chung, S. F. & Randolph, M. (2004) Penetration resistance in soft clay for different shaped penetrometers. In *Proceedings of the 2nd International Conference on Site Characterization*.) Millpress Science, vol. 1, pp. 671-677.

Cocjin, M., Gourvenec, S., White, D. & Randolph, M. (2014) Tolerably mobile subsea foundations – observations of performance. *Géotechnique* **64(11)**:895-909.

Colreavy, C., O'loughlin, C. D. & Randolph, M. (2016) Experience with a dual pore pressure element piezoball. *International Journal of Physical Modelling in Geotechnics* **16(3)**:101-118.

De Catania, S., Breen, J., Gaudin, C. & White, D. J. (2010) Development of a multiple-axis actuator control system. In *Physical Modelling in Geotechnics, Two Volume Set*.) CRC Press, pp. 325-330.

Dingle, H. R. C., White, D. J. & Gaudin, C. (2008) Mechanisms of pipe embedment and lateral breakout on soft clay. *Canadian Geotechnical Journal* **45(5)**:636-652.

Einav, I. & Randolph, M. F. (2005) Combining upper bound and strain path methods for evaluating penetration resistance. *International Journal for Numerical Methods in Engineering* **63(14)**:1991-2016.

Feng, X. & Gourvenec, S. (2015) Consolidated undrained load-carrying capacity of subsea mudmats under combined loading in six degrees of freedom. *Géotechnique* **65(7)**:563-575.

Gaudin, C., White, D. J., Boylan, N., Breen, J., Brown, T., De Catania, S. & Hortin, P. (2009) A wireless high-speed data acquisition system for geotechnical centrifuge model testing. *Measurement Science and Technology* **20(9)**:095709.

Gourvenec, S., Acosta-Martinez, H. & Randolph, M. (2009) Experimental study of uplift resistance of shallow skirted foundations in clay under transient and sustained concentric loading. *Géotechnique* **59(6)**:525-537.

Gourvenec, S. M., Vulpe, C. & Murthy, T. G. (2014) A method for predicting the consolidated undrained bearing capacity of shallow foundations. *Géotechnique* **64(3)**:215-225.

Hill, A. J., White, D. J., Bruton, D. a. S., Langford, T., Meyer, V., Jewell, R. & Ballard, J. C. (2012) A new framework for axial pipe-soil resistance, illustrated by a range of marine clay satasets. In *7th Int. Conf. on Offshore Site Investigation and Geotechnics*.) Society of Underwater Technology, London.

Krost, K., Gourvenec, S. M. & White, D. J. (2011) Consolidation around partially embedded seabed pipelines. *Géotechnique* **61(2)**:167-173.

Low, H., Randolph, M. & Kelleher, P. (2007) Comparison of pore pressure generation and dissipation rates from cone and ball penetrometers. In *Offshore Site Investigation - Confronting New Challenges and Sharing Knowledge*.) Society for Underwater Technology, vol. n/a, pp. 547-556.

Low, H. E., Lunne, T., Andersen, K. H., Sjursen, M. A., Li, X. & Randolph, M. F. (2010) Estimation of intact and remoulded undrained shear strengths from penetration tests in soft clays. *Géotechnique* **60(11)**:843-859.

Martin, C. M. & Randolph, M. F. (2006) Upper-bound analysis of lateral pile capacity in cohesive soil. *Géotechnique* **56(2)**:141-145.

Martin, C. M. & White, D. J. (2012) Limit analysis of the undrained bearing capacity of offshore pipelines. *Géotechnique* **62(9)**:847-863.

Merifield, R., White, D. & Randolph, M. (2009) Effect of Surface Heave on Response of Partially Embedded Pipelines on Clay. *Journal of Geotechnical and Geoenvironmental Engineering* **135(6)**:819-829.

Merifield, R., White, D. J. & Randolph, M. F. (2008) The ultimate undrained resistance of partially embedded pipelines. *Géotechnique* **58(6)**:461-470.

Murff, J. D., Wagner, D. A. & Randolph, M. F. (1989) Pipe penetration in cohesive soil. *Géotechnique* **39(2)**:213-229.

Randolph, M. & Hope, S. (2004) Effect of cone velocity on cone resistance and excess pore pressures. In *Proceedings of the IS Osaka - Engineering Practice and Performance of Soft Deposits*.) Yodogawa Kogisha Co. Ltd, pp. 147-152.

Randolph, M. F. & Houlsby, G. T. (1984) The limiting pressure on a circular pile loaded laterally in cohesive soil. *Géotechnique* **34(4)**:613-623.

Randolph, M. F., Jewell, R. J., Stone, K. J. & Brown, T. A. (1991) Establishing a new centrifuge facility. In *international conference on centrifuge modelling, Centrifuge '91*. (Ko, H.-Y., andMclean, F. G. (eds)) Balkema, Boulder pp. 3–9.

Randolph, M. F. & White, D. J. (2008) Upper-bound yield envelopes for pipelines at shallow embedment in clay. *Géotechnique* **58(4)**:297-301.

Randolph, M. F., White, D. J. & Yan, Y. (2012) Modelling the axial soil resistance on deep-water pipelines. *Géotechnique* **62(9)**:837-846.

Sinclair, F., Carr, M., Bruton, D. & Farrant, T. (2009) Deesign challenges and experience with controlled lateral buckle initiation methods In *Proceedings of 28th International Conference on Ocean, Offshore and Arctic Engineering*. ASME vol. 3, pp. 319-330.

Wang, D., White, D. J. & Randolph, M. F. (2010) Large-deformation finite element analysis of pipe penetration and large-amplitude lateral displacement. *Canadian Geotechnical Journal* **47(8)**:842-856.

White, D. J. & Randolph, M. F. (2007) Seabed characterisation and models for pipeline-soil interaction. *International Journal of Offshore and Polar Engineering* **7(3)**:193-204.

Table 1 Pipe test s programme

Test name	Initial penetration, *w/D*	Recorded max. penetration resistance, V_{max}: kN/m	Vertical load ratio, V_{op}/V_{max} during post-lay consolidation	Vertical installation	Consolidation prior to break-out	Loading conditions
Axial breakout						
R4UU_AX	0.5	2.8	0.25	Monotonic	No	§
R4CU_AX		2.4	0.25		Yes	†
Lateral breakout						
R4UU	0.5	2.9	0.25	Monotonic	No	§
R8UU		2.7	0.125		No	§
R1CU		2.7	1		Yes	†
R2CU		2.6	0.5		Yes	†
R4CU		2.6	0.25		Yes	†
R8CU		2.9	0.125		Yes	†
RemR4CU		1.9	0.25	Cyclic with oscillations in *x* direction	Yes	‡

Detailed test procedure

§ - Monotonic penetration to *w/D* (V_{max}) → Unload to V_{op}/V_{max} → Breakout

† - Monotonic penetration to *w/D* (V_{max}) → Unload to V_{op}/V_{max} →Consolidate → Breakout

‡ - Cyclic penetration to *w/D* (V_{max}) → Unload to V_{op}/V_{max} →Consolidate → Breakout

Figures

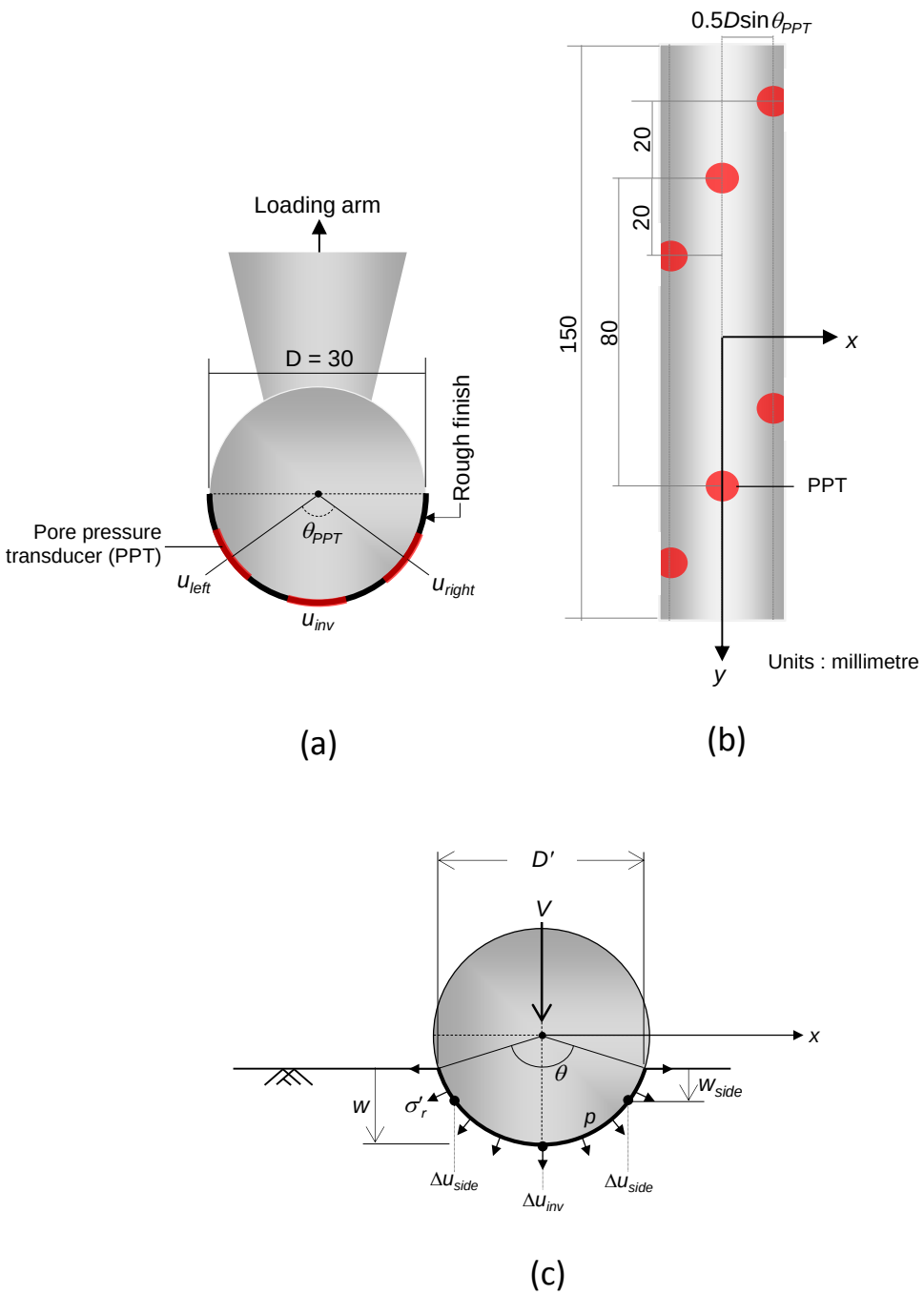

Figure 1 Schematic drawing of model pipe: in (a) transverse and (b) plan view; and (c) idealisation of loads acting on the pipe

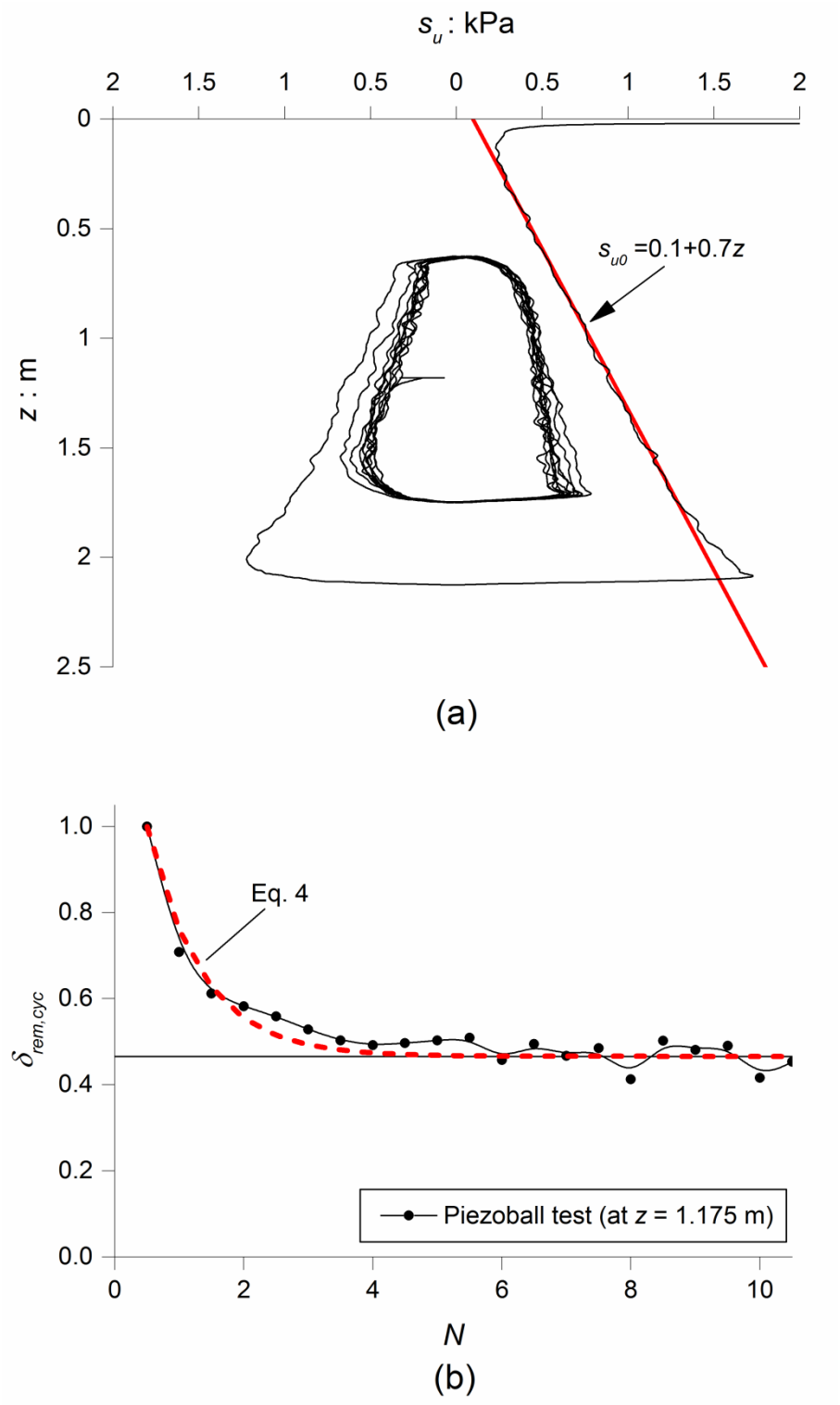

Figure 2 Characterisation of the soil model using a ball penetrometer showing: (a) undrained shear strength, s_u with depth, z (prototype scale), and (b) degradation of soil strength during cyclic penetrometer test plotted in terms of remoulded strength ratio, $\delta_{rem,cyc} = s_{u,cyc}/s_{u0}$ against cycle number, N

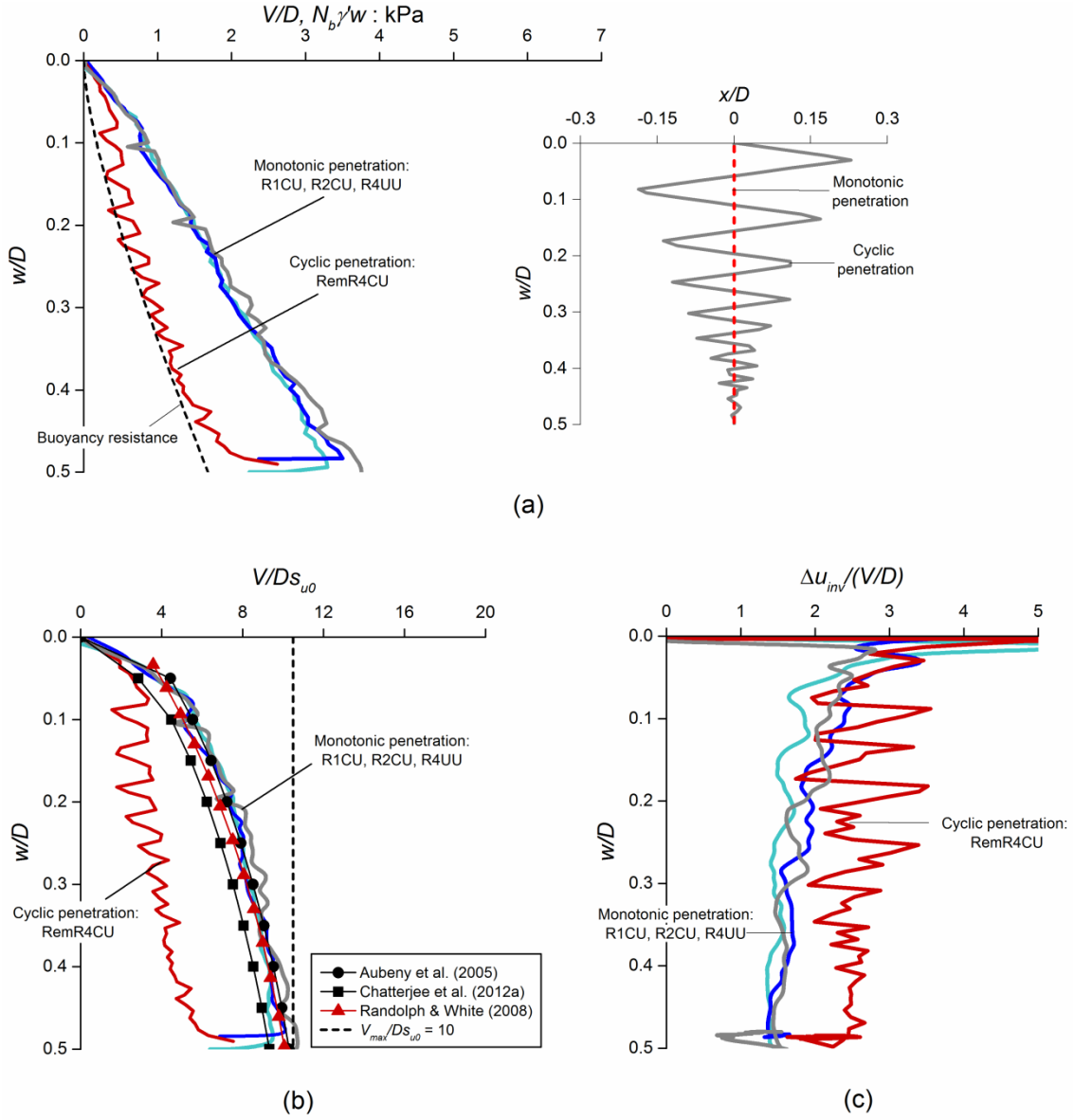

Figure 3 Undrained pipe penetration response showing: (a) buoyancy resistance, $N_b\gamma'w$ and vertical bearing pressure per unit length, V/D; (b) normalised vertical penetration resistance, V/Ds_{u0}; and (c) excess pore water pressure at the pipe invert normalised by vertical bearing pressure per unit length, $\Delta u_{inv}/(V/D)$, plotted against the normalised pipe embedment at the invert level, w/D, during penetration (inset in (a): pipe displacement in lateral and vertical directions (x/D – w/D) during monotonic and cyclic penetration)

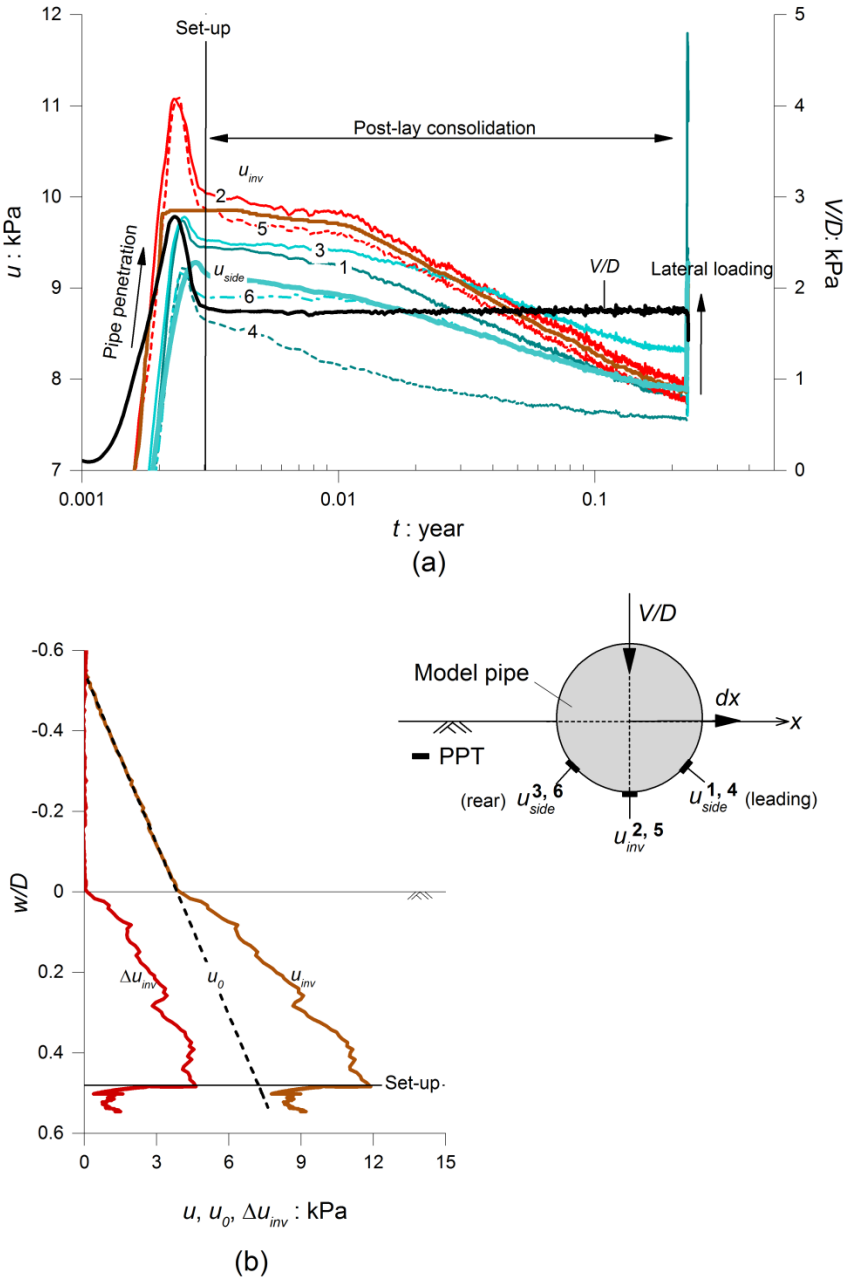

478

479 **Figure 4** Variation in pore water pressure along the embedded pipe in test R2CU, showing: (a)
480 pore water pressure, u measured at different pore pressure transducers (PPTs), and penetration
481 resistance V/D, during the whole test, plotted against time, t in prototype scale; (b) hydrostatic
482 pore water pressure, u_0 , and pipe invert record of pore water pressure, u_{inv}, and excess pore water
483 pressure, Δu_{inv}, plotted against normalised pipe embedment at the invert level, w/D during
484 penetration

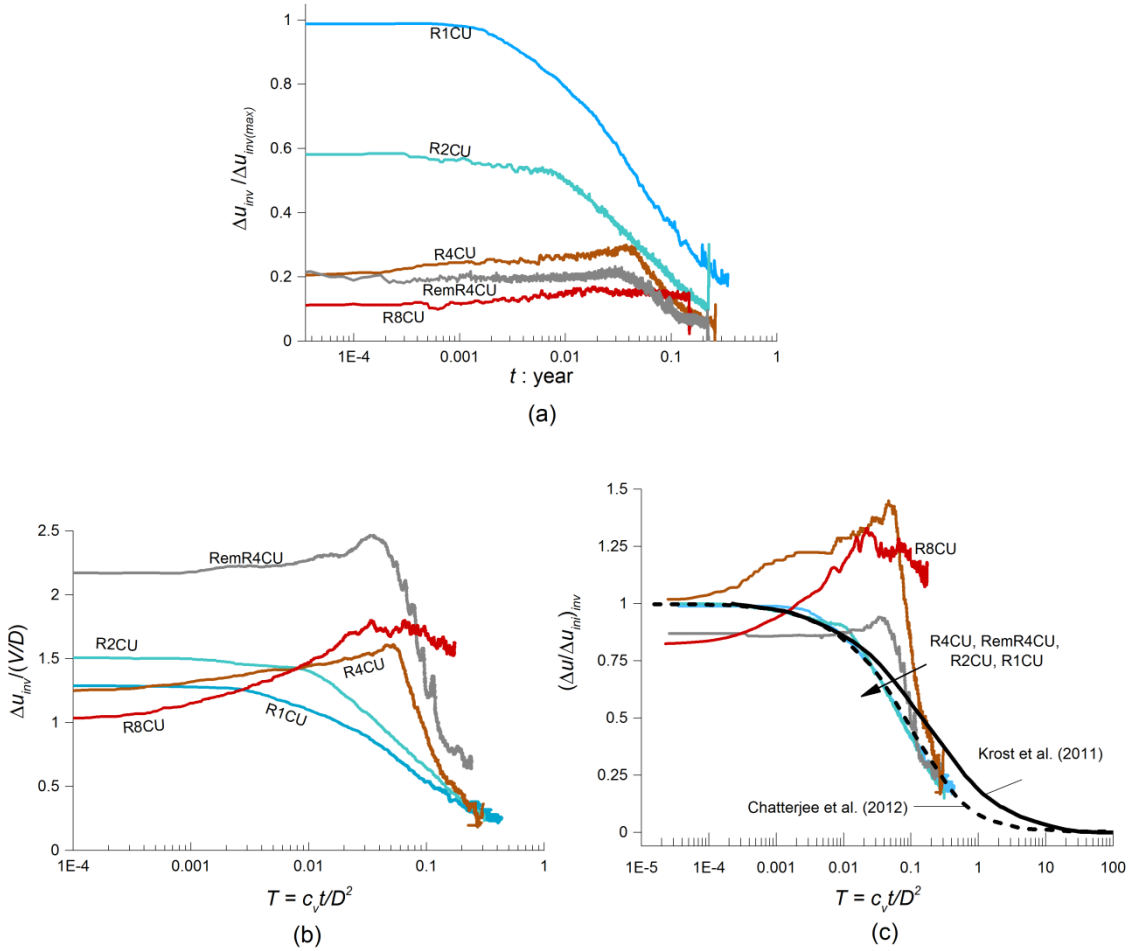

485

Figure 5 Dissipation-time histories of excess pore pressure at the pipe invert, Δu_{inv} during consolidation: (a) normalised by initial excess pore pressure at maximum vertical load, $\Delta u_{inv\ (max)}$ plotted against time, t in prototype scale; (b) normalised by penetration resistance, V/D plotted against time factor, $T = c_v t/D^2$ and (c) normalised by initial excess pore pressure under operative consolidation load, $(\Delta u_{ini})_{inv}$ plotted against time factor, $T = c_v t/D^2$, where $t = 0$ at the moment when the reduction in vertical load is complete

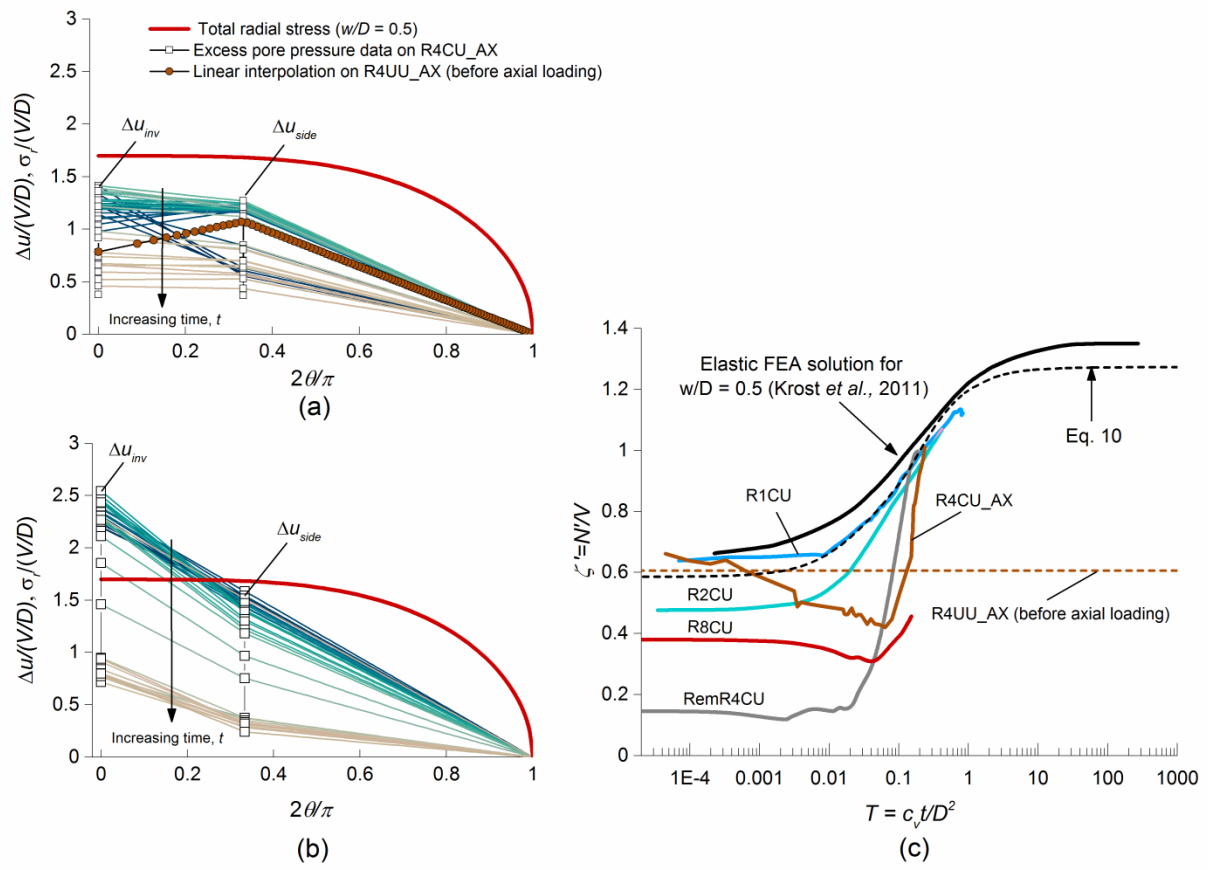

Figure 6 Effect of consolidation on pipe-soil contact stresses showing distribution of the total radial stress, σ_r and the interpolated excess pore pressure, Δu normalised by the prescribed vertical bearing pressure, V/D during tests (a) R4CU_AX, and R4UU_AX (before axial loading) and (b) RemR4CU, and (c) increase in effective contact enhancement factor, ζ' with time expressed as time factor, $T = c_v t/D^2$

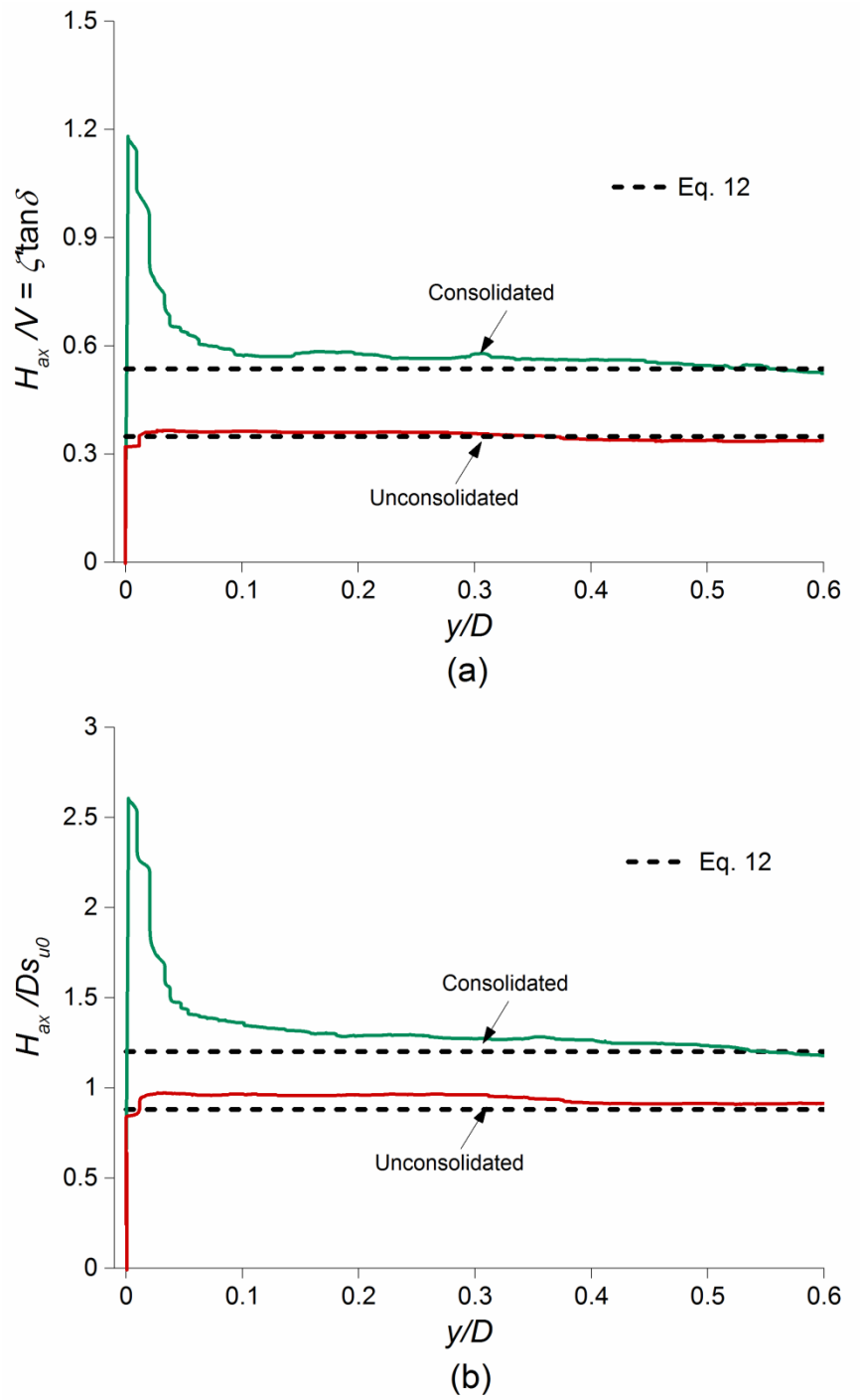

Figure 7 Effect of consolidation on axial pipe resistance showing: (a) axial friction factor, H_{ax}/V and (b) normalised axial breakout resistance, H_{ax}/Ds_{u0}, plotted against normalised axial displacement, y/D

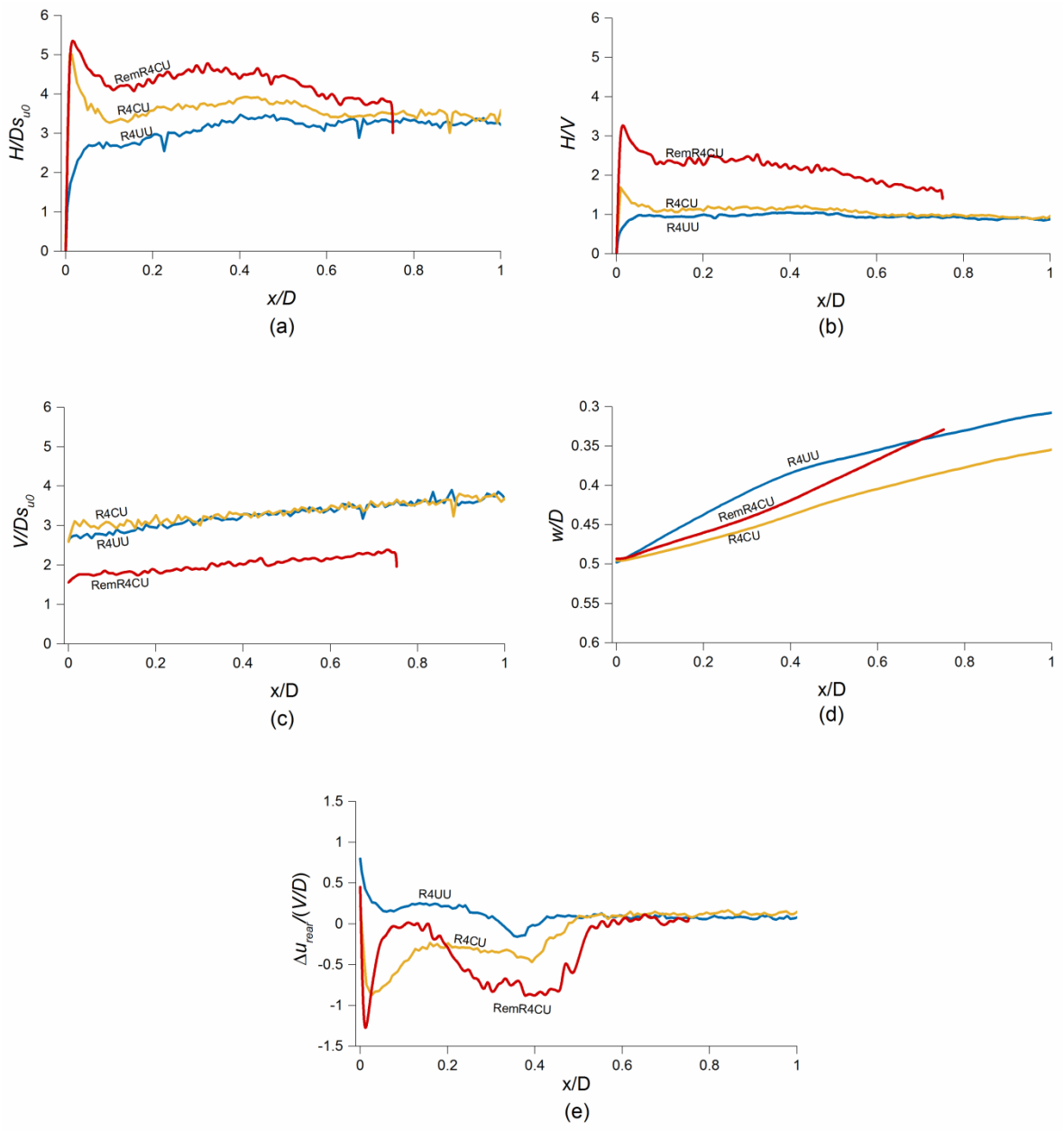

Figure 8 Effect of installation and post-lay consolidation on the lateral breakout resistance, showing (a) lateral resistance normalised by the in situ, undrained shear strength at the level of the pipe invert, H/Ds_{u0} (s_{u0} not constant), (b) lateral friction factor, H/V, (c) normalised vertical resistance, V/Ds_{u0}, (d) normalised pipe invert elevation, w/D, and (e) excess pore pressure at the rear face of the pipe, Δu_{rear} normalised by the vertical bearing pressure per unit length, V/D, plotted against normalised lateral displacement, x/D for tests with operative vertical load ratios, V_{op}/V_{max} = 0.25 (R4 series)

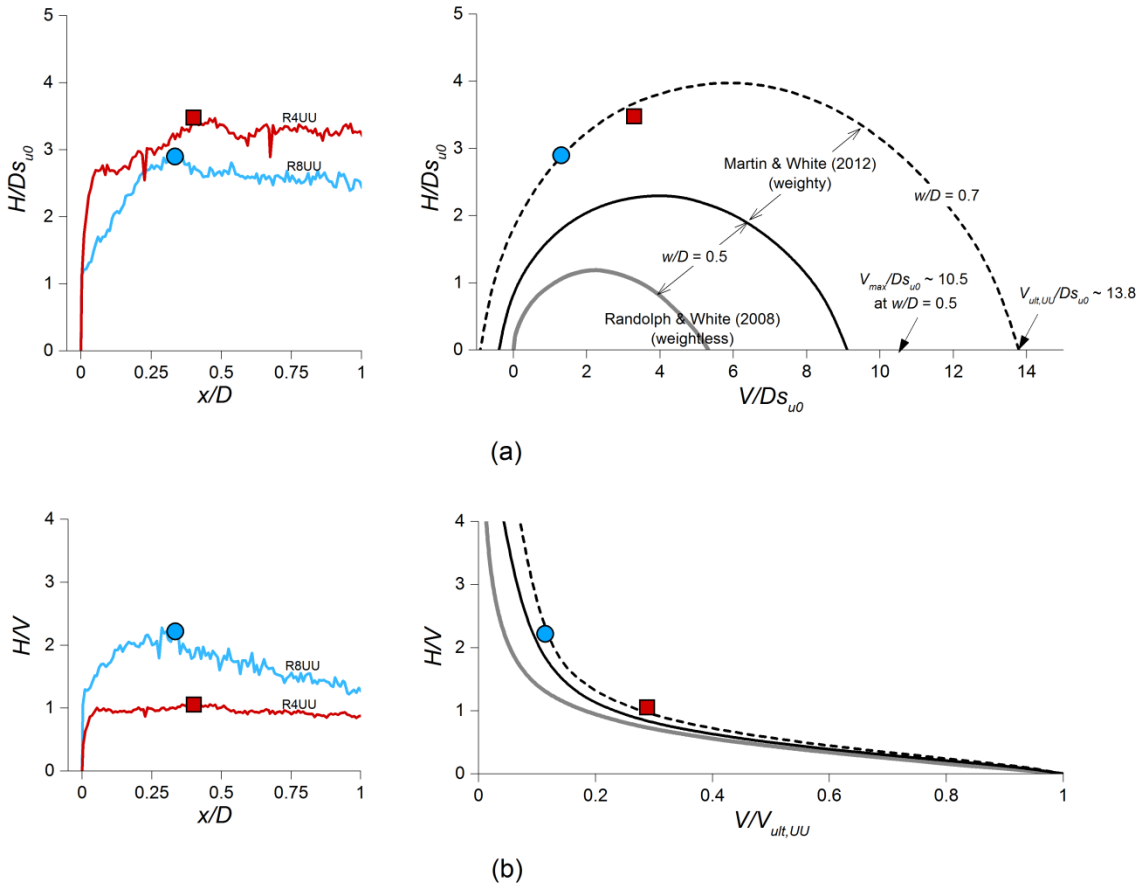

Figure 9 Unconsolidated lateral breakout responses, showing: (a) normalised lateral resistance, H/Ds_{u0}, and (b) lateral friction factor, H/V responses, relative to theoretical failure envelopes

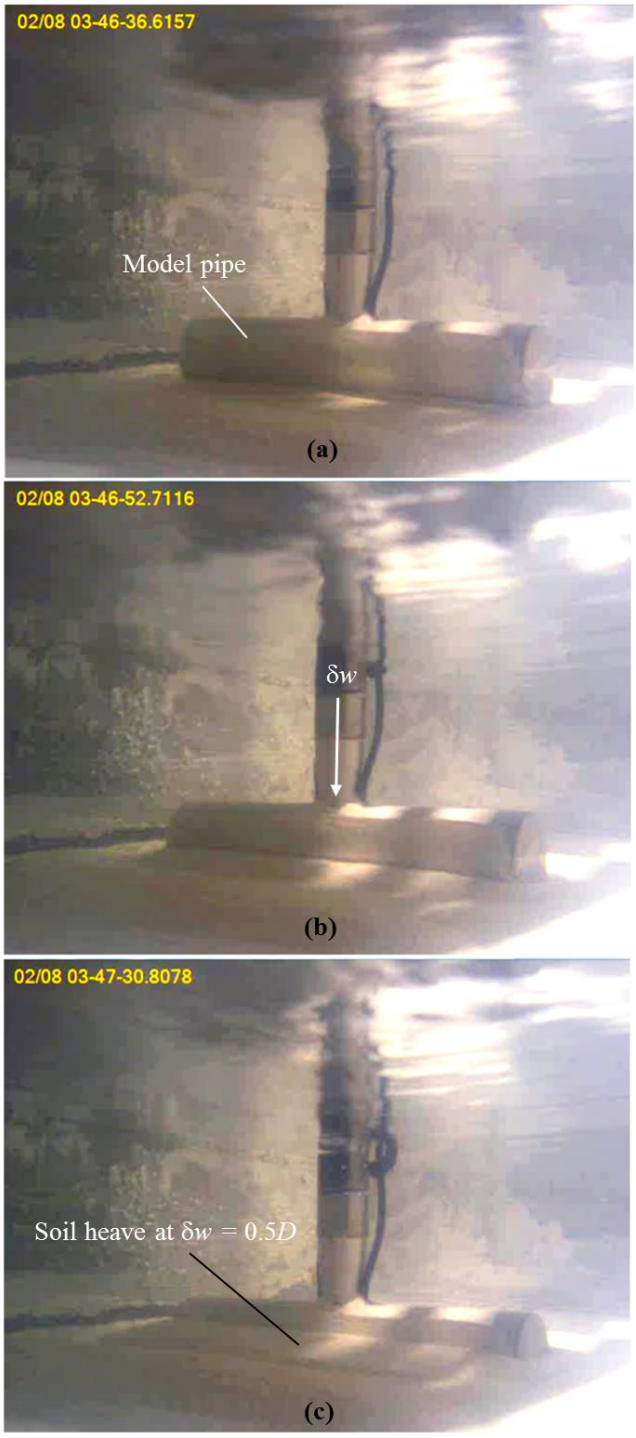

Figure 10 Development of soil heave during pipe penetration, shown by a sequence of test photos in the following order: (a) before penetration, (b) during penetration, and (c) at maximum penetration

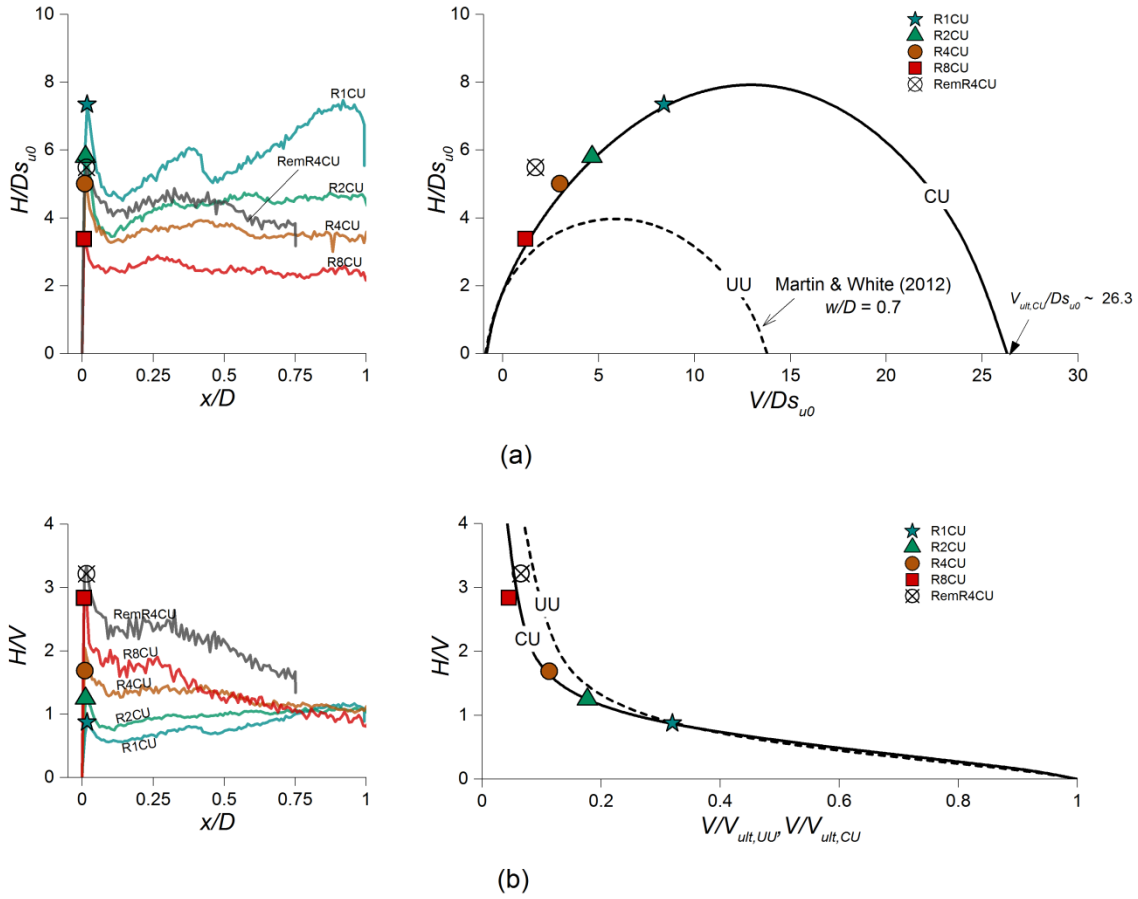

Figure 11 Consolidated lateral breakout responses, showing: (a) normalised lateral resistance, H/Ds_{u0}, and (b) lateral friction factor, H/V responses, relative to theoretical failure envelopes

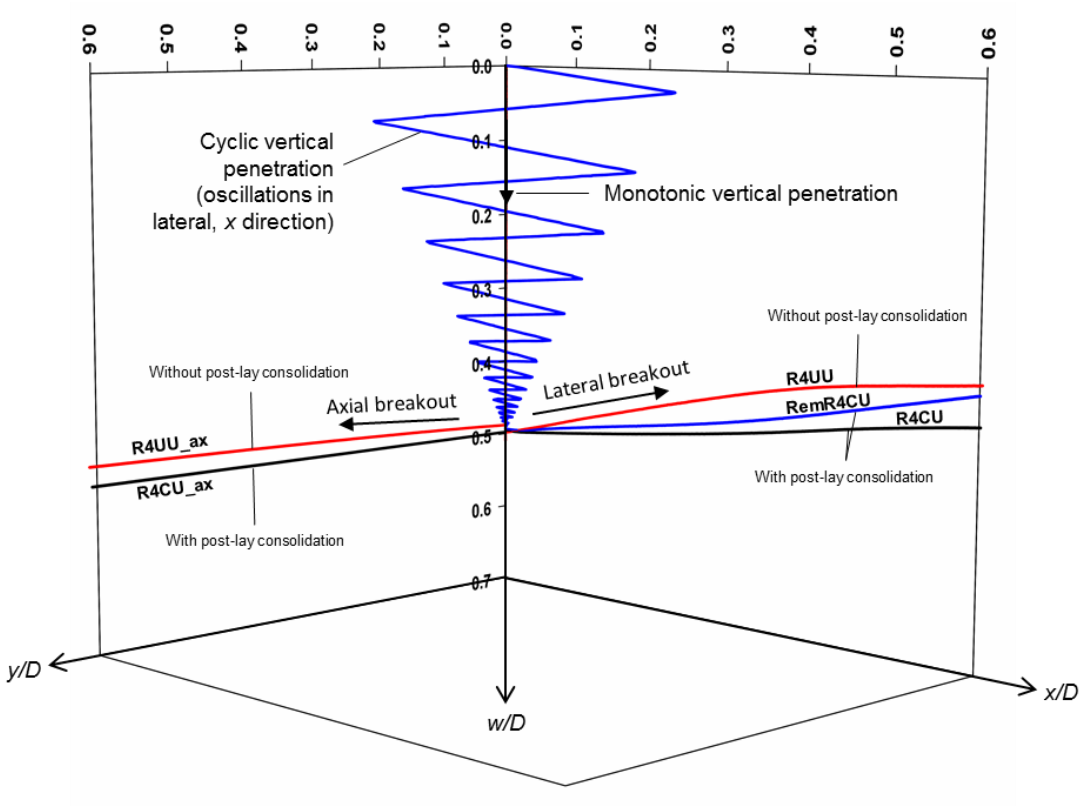

Figure 12 Effect of consolidation on pipe trajectory during axial and lateral loading shown in three-dimensional normalised (*x/D*, *y/D*, *w/D*) space

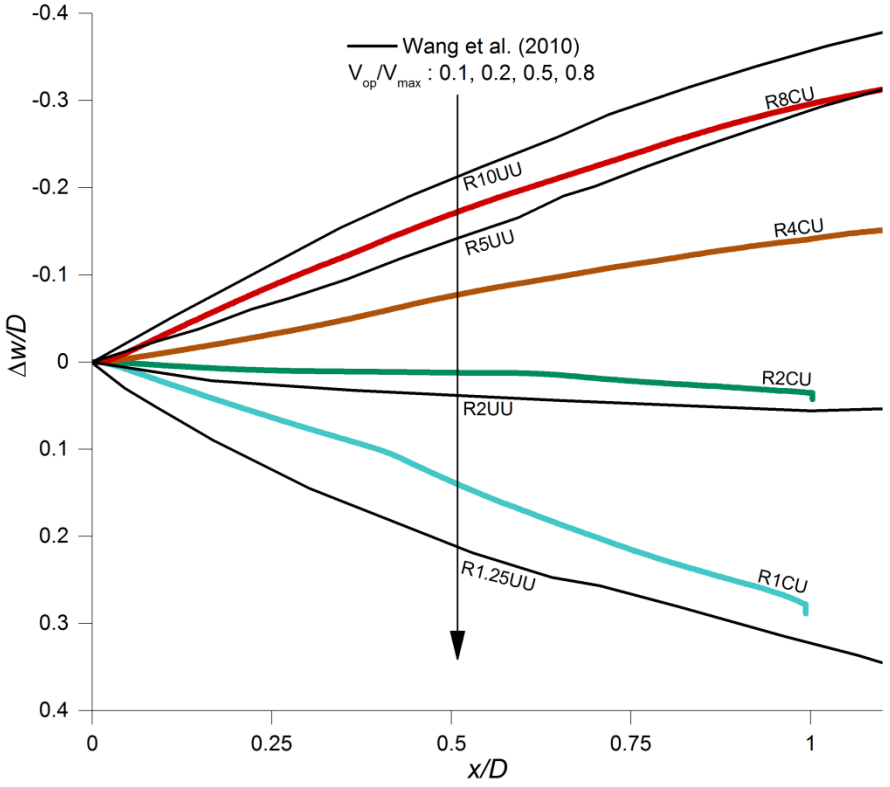

Figure 13 Effect of pipe weight on the pipe trajectory during lateral breakout

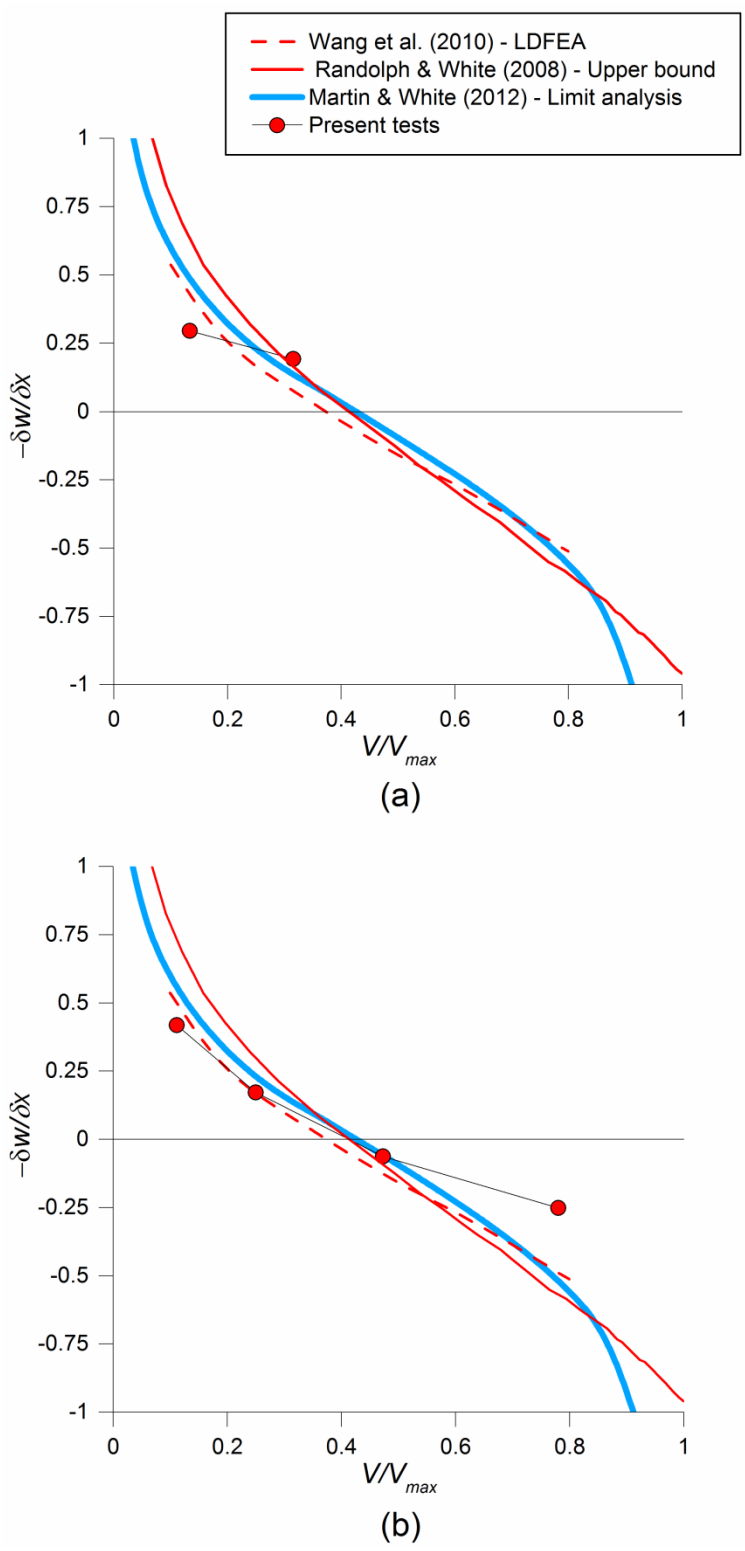

Figure 14 Inclination of displacement paths at lateral breakout compared against existing solutions , shown for: (a) cases without post-lay consolidation, and (b) cases with post-lay consolidation